Kinetic signatures of myosin-5B, the motor involved in microvillus inclusion disease

Received for publication, June 9, 2017, and in revised form, August 29, 2017 Published, Papers in Press, September 7, 2017, DOI 10.1074/jbc.M117.801456

Sarah M. Heissler[‡1], **Krishna Chinthalapudi**[§], **and James R. Sellers**[‡2]

From the [‡]*Laboratory of Molecular Physiology, NHLBI, National Institutes of Health, Bethesda, Maryland 20892-8015 and the* [§]*Cell Adhesion Laboratory, Department of Integrative Structural and Computational Biology, Scripps Research Institute, Jupiter, Florida 33458*

Edited by Joseph Jez

Myosin-5B is a ubiquitous molecular motor that transports cargo vesicles of the endomembrane system in intracellular recycling pathways. Myosin-5B malfunction causes the congenital enteropathy microvillus inclusion disease, underlining its importance in cellular homeostasis. Here we describe the interaction of myosin-5B with F-actin, nucleotides, and the pyrazolopyrimidine compound myoVin-1. We show that single-headed myosin-5B is an intermediate duty ratio motor with a kinetic ATPase cycle that is rate-limited by the release of phosphate. The presence of a second head generates strain and gating in the myosin-5B dimer that alters the kinetic signature by reducing the actin-activated ADP release rate to become rate-limiting. This kinetic transition into a high-duty ratio motor is a prerequisite for the proposed transport function of myosin-5B in cellular recycling pathways. Moreover, we show that the small molecule compound myoVin-1 inhibits the enzymatic and functional activity of myosin-5B *in vitro*. Partial inhibition of the actin-activated steady-state ATPase activity and sliding velocity suggests that caution should be used when probing the effect of myoVin-1 on myosin-5–dependent transport processes in cells.

Double-headed class 5 myosins are evolutionary ancient, prototypic actin-based molecular motors implicated in the spatiotemporal segregation and the transport of organelles across phylogeny (1–10). A prerequisite for efficient transport is that a single motor can either take multiple discrete steps on an actin filament without detaching, a property also referred to as processivity, or that the motor works in an ensemble with other myosins-5 to efficiently move a cargo. These differences in physiological capacities and limitations are directly linked to the mechanoenzymatic signatures of class 5 myosins (11, 12).

This work was supported by the Intramural Research Program of the National Heart, Lung, and Blood Institute of the National Institutes of Health (HL004229). The authors declare that they have no conflicts of interest with the contents of this article. The content is solely the responsibility of the authors and does not necessarily represent the official views of the National Institutes of Health.

[1] To whom correspondence may be addressed: Laboratory of Molecular Physiology, NHLBI, National Institutes of Health, 50 South Dr., B50/3529, Bethesda, MD 20892-8015. Tel.: 301-496-8010; Fax: 301-402-1519; E-mail: sarah.heissler@nih.gov.

[2] To whom correspondence may be addressed: Laboratory of Molecular Physiology, NHLBI, National Institutes of Health, 50 South Dr., B50/3523, Bethesda, MD 20892-8015. Tel.: 301-496-6887; Fax: 301-402-1519; E-mail: sellersj@nhlbi.nih.gov.

Mammals express three myosin-5 genes (*MYO5A*, *MYO5B*, and *MYO5C*) in almost all cells (6, 13). Compared with the well studied paralog myosin-5A that exhibits single molecule processivity and the nonprocessive myosin-5C, little is known about the kinetic features of myosin-5B (14–18). Myosin-5B is best known for the transport of Rab GTPase positive vesicles of the endomembrane system along the F-actin cytoskeleton to the plasma membrane (4, 19–21). The long-range vesicle transport system is a prerequisite for diverse physiological processes including axon development, postsynaptic plasticity, cell polarization, and the prevention of polyspermy (19, 22–25). The mutation-induced loss of function of *MYO5B* is manifested in debilitating pathologies including microvillus inclusion disease that results in death in neonates and children (20, 26, 27). As reviewed recently, the majority of the >40 disease-associated mutations in *MYO5B* cluster in the coding region for the motor and the tail domain of the myosin heavy chain (26). The motor domain harbors a prototypic nucleotide-binding pocket and a binding region for F-actin (Fig. 1*A*). The tail domain contains a coiled-coil region that promotes the dimerization of two myosin heavy chains and terminates in a distal globular tail domain that constitutes the binding site for Rab GTPase family members and other adaptor proteins (4, 13, 25, 28). Both domains are separated by the neck that contains six IQ motifs, predicted binding regions for calmodulin (CaM)[3] or calmodulin-like light chains (Fig. 1*A*) (29, 30). The distribution of mutations in the myosin heavy chain suggests that either (i) the nucleotide-dependent interaction between the motor domain and the actin filament may be altered or (ii) the interaction between the molecular motor and its cargo vesicle may be altered. Both scenarios are expected to result in the aberrant vesicle trafficking patterns in patients with microvillus inclusion disease (31, 32).

To understand the mechanoenzymatic basis of the actin-based transport powered by myosin-5B in normalcy, we studied the interaction between the motor, nucleotides, and F-actin (Fig. 1*B*) with ensemble solution kinetics and functional assays *in vitro*. Our experiments show that single-headed myosin-5B has an intermediate duty ratio and that a second head is required to establish a high-duty ratio, a kinetic prerequisite for single molecule processivity. The data also allows for the comparative analysis of kinetic signatures in the class 5 myosome. Moreover, we show that the small molecule myoVin-1 inhibits

[3] The abbreviation used is: CaM, calmodulin.

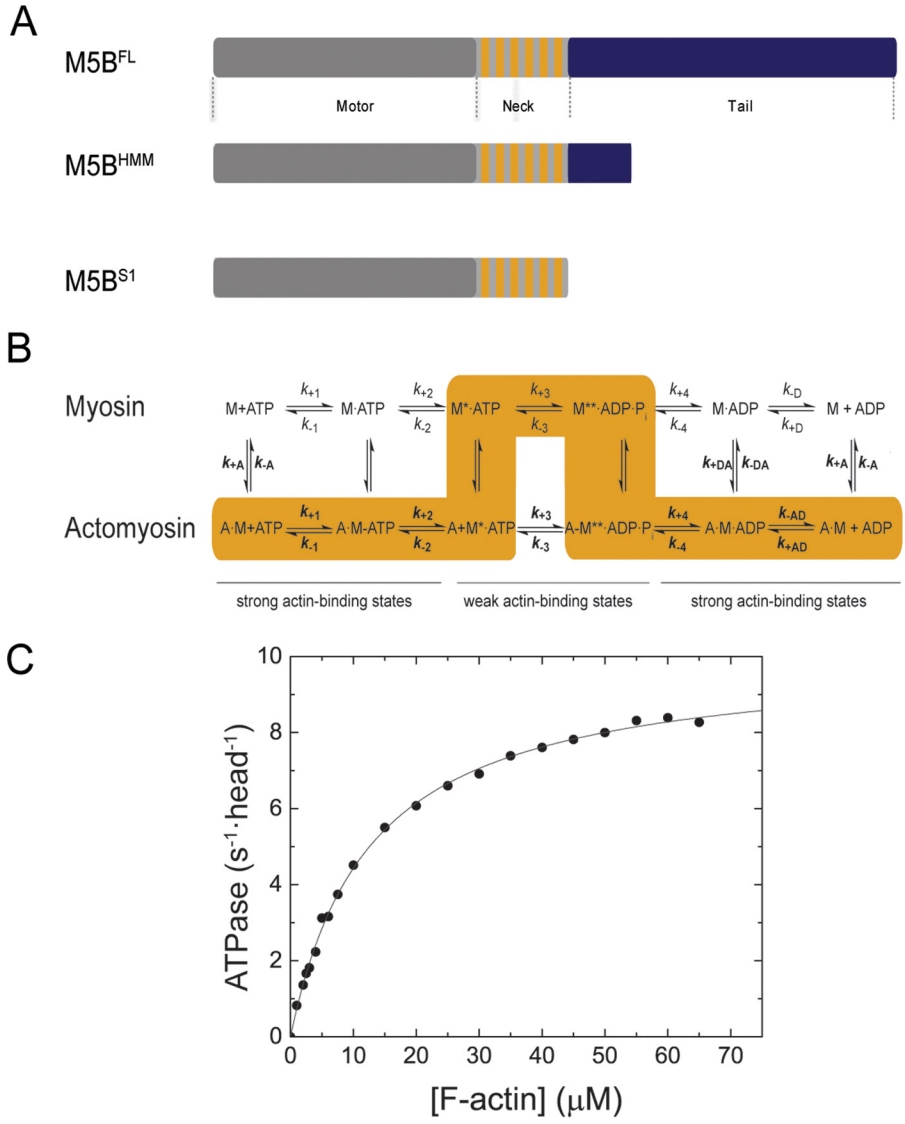

Figure 1. Domain organization, kinetic scheme, and steady-state ATPase activity of M5B^{S1}. *A*, domain organization of myosin-5B and expression constructs used in this work. The myosin motor domain in the myosin heavy chain is shown in *gray*. The six IQ motifs in the myosin neck domain are shown in *orange*, and the tail domain is in *blue*. The tail domain mediates the dimerization of M5B^{FL} and M5B^{HMM} by means of a coiled-coil and interacts with binding partners. *B*, simplified kinetic scheme of the myosin and actomyosin ATPase cycle. The events of ATP binding, ATP hydrolysis, and phosphate release are shown for myosin in the actin detached (*top row*) and attached (*bottom row*) states. The main flux through the pathway is highlighted in *orange*, and the weak and strong actin-binding states are indicated. The notation distinguishes between the kinetic constants in the presence and absence of F-actin by using *regular versus bold type*; subscripts *A* and *D* refer to F-actin ($\boldsymbol{K_A}$) and ADP (K_D), respectively. Dissociation equilibrium constants were calculated as $K_x = k_{-x}/k_{+x}$. *M*, myosin; *A*, actin. *C*, steady-state ATPase activity of M5B^{S1}. Increasing concentrations of F-actin activate the steady-state ATPase activity to a k_{cat} of 10.0 ± 0.1 s^{-1} with a K_{app} of 12.6 ± 0.4 μM.

the enzymatic and functional activity of myosin-5B *in vitro*. The observed effects resemble the previously described effect on myosin-5A and suggest that myoVin-1 may inhibit all class 5 myosins.

Results

Design of expression constructs for kinetic experiments

We recombinantly overproduced and purified the single-headed M5B^{S1} that contains all six IQ motifs and the double-headed M5B^{HMM} (Fig. 1*A*) in complex with the light chain CaM in milligram quantities in the baculovirus/*Sf*9 insect cell system. The proteins allowed us to directly compare the mechanoenzymatic properties of single-headed and double-headed myosin-5B constructs and their interaction with nucleotides, F-actin, and the small molecule myoVin-1.

Enzymatic activity of M5B^{S1} under steady-state conditions

We first determined the enzymatic activity of M5B^{S1} with an NADH-coupled assay under steady-state conditions. As shown in Fig. 1*C*, F-actin potently activates the basal ATPase activity of M5B^{S1} from a k_{basal} of 0.07 ± 0.01 s^{-1} more than 2 orders of magnitude. Fitting a Michaelis–Menten equation

$$k_{obs} = \frac{k_{cat}[\text{F–actin}]}{K_{app} + [\text{F–actin}]} \qquad \text{(Eq. 1)}$$

to the data results in a k_{cat} of 10.0 ± 0.1 s^{-1}. The K_{app} is 12.6 ± 0.4 μM, the catalytic efficiency k_{cat}/K_{app} ~0.8 μM^{-1} s^{-1}. The steady-state kinetic parameters of M5B^{S1} are compiled in Table 1 and compared with previously studied class 5 myosins.

Table 1
Steady-state kinetic parameters of mouse M5B^{S1} in comparison with previously characterized class-5 myosins
ND, not determined.

Steady-state ATPase parameter	Signal or calculation	*Mm* M5B^{S1}[a]	*Gg* M5A^{S1} (35)	*Hs* M5C^{S1} (16)	*Dm* M5^{S1} (47)
k_{basal} (s^{-1})	NADH assay	0.07 ± 0.01	0.03	0.05 ± 0.01	ND
k_{cat} (s^{-1})	NADH assay	10.0 ± 0.1	15	1.8 ± 0.3	12.5 ± 0.8
K_{app} (μM)	NADH assay	12.6 ± 0.4	1.4	42.5 ± 10.6	9.9 ± 0.6
k_{cat}/K_{app} ($\mu M^{-1}\ s^{-1}$)	NADH assay	~0.8	~11	~0.04	~1.3

[a] In this study.

ATP binding to myosin

To determine the rate-limiting step of the M5B^{S1} kinetic cycle, we measured the individual parameters that describe the events of ATP binding, ATP hydrolysis and product release in the F-actin attached and detached states (Fig. 1*B*) in a stopped-flow spectrophotometer. As shown in the *inset* of Fig. 2*A*, ATP binding to M5B^{S1} causes a transient increase in the intrinsic tryptophan fluorescence that is best described by a single exponential fit. The observed rate constants k_{obs}, obtained by varying the ATP concentration, follow a hyperbolic dependence according to

$$k_{obs} = \frac{[ATP]k_{max}}{[ATP] + K_{0.5}} \quad \text{(Eq. 2)}$$

and approach a maximum k_{max} value of 85.4 ± 1.5 s^{-1}, representing the ATP hydrolysis rate $k_{+3} + k_{-3}$. Half-saturation ($1/K_{0.5}$) is observed at an ATP concentration of 225.1 ± 14.7 μM (Fig. 2*A*). At low ATP concentrations, the dependence of the observed rate constant on ATP is linear. The slope of the straight line yields the apparent second-order rate constant for ATP binding, $K_1k_{+2} = 0.39 \pm 0.01\ \mu M^{-1}{\cdot}s^{-1}$ (Fig. 2*B*). An identical value of 0.4 ± 0.01 $\mu M^{-1}\ s^{-1}$ is obtained after binding of the nucleotide analog mantATP to M5B^{S1} under pseudo-first order conditions. Fig. 2*B* shows the binding data of both nucleotides up to a concentration of 25 μM. All transient-state kinetic parameters of M5B^{S1} are compiled in Table 2 and compared with previously studied single-headed myosins-5.

ATP binding to actomyosin

The time-dependent change in light scattering signal was used to assay the interaction between actomyosin and ATP. Mixing of 0.3 μM actoM5B^{S1} with excess ATP results in a single exponential decrease in light scattering signal, as shown in the *inset* of Fig. 2*C*. The observed rate constant k_{obs} values follow a hyperbolic dependence as a function of ATP that is best described by the following equation.[4]

$$k_{obs} = \frac{[ATP]\boldsymbol{k_{+2}}}{[ATP] + \boldsymbol{K_{0.5}}} \quad \text{(Eq. 3)}$$

The fit converges toward a maximum $\boldsymbol{k_{+2}}$ value of 373.5 ± 18.7 s^{-1}. Half-saturation ($1/\boldsymbol{K_{0.5}} = 1/\boldsymbol{K_1}$) is observed at 745.6 ± 120.7 μM ATP (Fig. 2*C*). At low [ATP] up to 50 μM, the data set is best fit with a linear function, representing the apparent second-order binding rate constant $\boldsymbol{K_1k_{+2}} = 0.28 \pm 0.01\ \mu M^{-1}\ s^{-1}$ (Fig. 2*D*).

ADP binding and release from myosin

Binding kinetics of the fluorescent nucleotide analog mantADP to M5B^{S1} were determined in a stopped-flow spectrophotometer. Mixing of 0.5 μM M5B^{S1} under pseudo-first order conditions with mantADP results in a single exponential fluorescence increase (Fig. 3*A*, *inset*). A linear fit to the data set according to

$$k_{obs} = k_{+D}[ADP] + k_{-D} \quad \text{(Eq. 4)}$$

results in a second-order binding rate constant k_{+D} of 3.05 ± 0.16 $\mu M^{-1}\ s^{-1}$ (Fig. 3*A*). Extrapolation of the fit to [mantADP] = 0 determines the ADP release rate constant k_{-D} = 14.3 ± 1.61 s^{-1}. This value is an order of magnitude higher than for previously characterized class 5A myosins (Table 2). As an independent measure, we directly determined k_{-D} in chasing experiments in which mantADP is displaced from the myosin·mantADP complex with excess ATP. Independently, we measured the ADP release rate constant from the myosin·ADP complex when chased with excess ATP. The latter experimental design uses the intrinsic tryptophan fluorescence of myosin as readout. Both experimental setups result in almost identical values for k_{-D} of 18.0 ± 0.29 s^{-1} (mantADP) and 18.9 ± 0.09 s^{-1} (ADP) that are in good agreement to the determined value from the binding data (k_{-D} = 14.3 ± 1.61 s^{-1}) (Fig. 3*B* and Table 2). From the ratio of the ADP release and binding rate constants ($K_D = k_{-D}/k_{+D}$), the dissociation equilibrium constant of ADP was calculated to K_D = 4.7–6.2 μM.

ADP binding to actomyosin

ADP binding to the actomyosin complex was probed by mixing mantADP under pseudo-first order conditions with actoM5B^{S1}. The associated time-dependent fluorescence increase is best described by a single exponential fit (Fig. 3*C*). The plot of the observed rate constants k_{obs} *versus* [mantADP] follows a linear trend that is best described by the following equation.

$$k_{obs} = \boldsymbol{k_{+AD}}[ADP] + \boldsymbol{k_{-AD}} \quad \text{(Eq. 5)}$$

The slope of the line defines the ADP-binding rate constant $\boldsymbol{k_{+AD}}$ = 2.71 ± 0.11 $\mu M^{-1}\ s^{-1}$ (Fig. 3*C*). The ADP release rate constant $\boldsymbol{k_{-AD}}$ was extracted at [mantADP] = 0 to 21.9 ± 0.9 s^{-1} (Fig. 3*C*).

ADP release from actomyosin

The ADP release rate constant $\boldsymbol{k_{-AD}}$ was directly determined by chasing the actomyosin·ADP complex with excess ATP.

[4] The notation used throughout this article distinguishes between the kinetic constants in the presence and absence of F-actin by using regular (K1) versus bold (K1) type; subscripts A and D refer to F-actin ($\boldsymbol{K_A}$) and ADP (K_D), respectively.

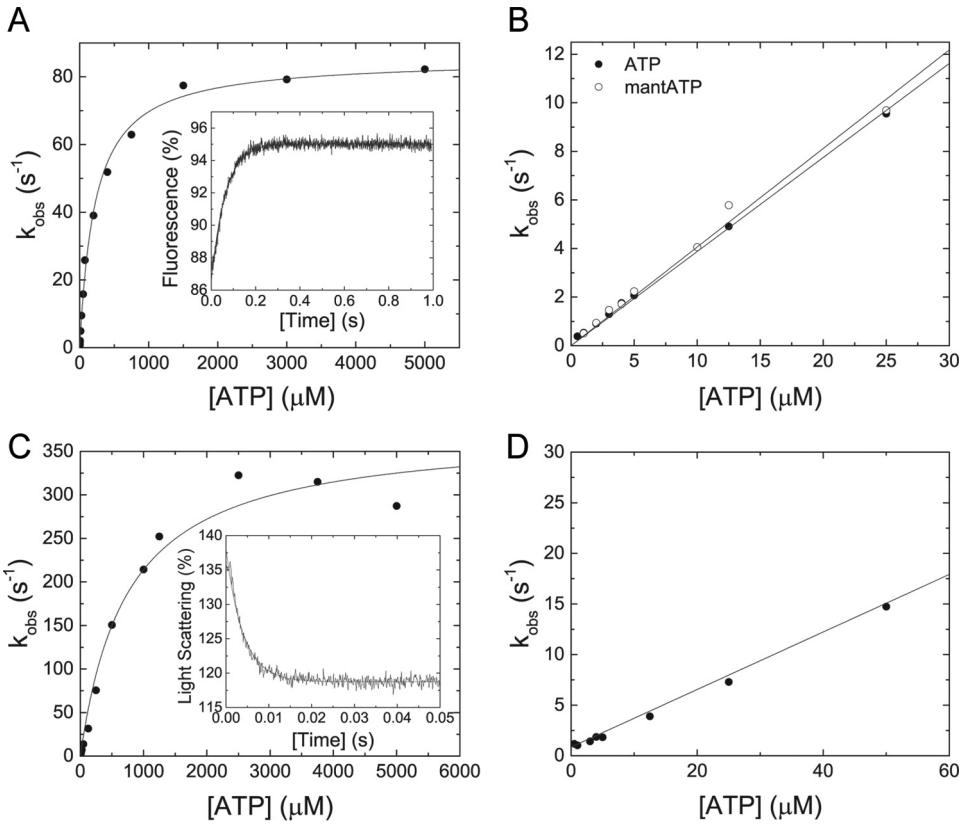

Figure 2. Transient kinetic interaction between MB5^{S1} and actoM5^{S1} with ATP and ATP analogs. *A*, the observed rate constant k_{obs} depends hyperbolically on the ATP concentration and converges a value $k_{+3} + k_{-3}$ of 85.4 ± 1.5 s^{-1}. Half-saturation ($1/K_{0.5}$) is reached at 225.1 + 14.7 μM ATP. *Inset*, the transient fluorescence increase represents the interaction between 50 μM ATP and 0.5 μM M5B^{S1} and has an observed rate constant k_{obs} of 15.84 s^{-1}. *B*, linear dependence of the observed rate constant k_{obs} on [ATP] at low nucleotide concentrations. Binding of ATP or the nucleotide analog mantATP results in identical second-order rate constants of 0.39 ± 0.01 and 0.4 ± 0.01 μM^{-1} s^{-1}, respectively. *C*, in the presence of F-actin, the observed rate constants k_{obs} of the ATP-induced dissociation of the actomyosin complex show a hyperbolic dependence on the ATP concentration and converge to a value $\boldsymbol{k_{+2}}$ of 373.5 ± 18.7 s^{-1} with half-saturation ($1/\boldsymbol{K_{0.5}} = 1/\boldsymbol{K_1}$) at 745.6 ± 120.7 μM ATP. *Inset*, time-dependent decrease in light scattering signal upon mixing 0.3 μM M5B^{S1} and 0.5 μM F-actin with 1250 μM ATP. The transient is best described with a single exponential fit with a k_{obs} of 252.22 s^{-1}. *D*, the observed rate constant k_{obs} of the ATP-induced dissociation of the actomyosin complex linearly depends on the ATP concentration up to 50 μM substrate, defining $\boldsymbol{K_1 k_{+2}}$ to 0.28 ± 0.01 μM^{-1} s^{-1}.

Two different experimental strategies were employed. First, mantADP was chased from actomyosin. Second, the change in light scattering upon the ATP-induced dissociation of the actomyosin·ADP complex was detected. In this indirect experimental setup, the ADP release limits the dissociation of the actomyosin complex. The former results in an ADP release rate $\boldsymbol{k_{-AD}}$ of 16.69 ± 0.11 s^{-1}, and the latter results in a $\boldsymbol{k_{-AD}}$ of 17.13 ± 0.14 s^{-1} (Fig. 3*D*). These independent measurements suggest that the fast ADP release rate is a kinetic signature of actoM5B^{S1}. The kinetic coupling ratio, the efficiency of F-actin to activate the ADP release, $\boldsymbol{k_{-AD}}/k_{-D}$ = ~1–1.5, is low. Accordingly, the dissociation equilibrium constant $\boldsymbol{K_{AD}} = \boldsymbol{k_{-AD}}/\boldsymbol{k_{+AD}}$ = 6.1–8.1 μM is similar to the respective constant in the absence of F-actin (K_D = 4.7–6.2 μM; Table 2).

Interaction with F-actin

The binding kinetics of M5B^{S1} to F-actin in the presence and absence of excess ADP was probed by light scattering. The transients are best described with single exponential fits as exemplarily shown in the *inset* of Fig. 4*A*. The obtained k_{obs} increase linearly within the F-actin concentration range tested. Linear fit of the data to

$$k_{obs} = \boldsymbol{k_{+DA}}[\text{F–actin}] + \boldsymbol{k_{-DA}} \quad \text{(Eq. 6)}$$

results in the second-order binding rate constants $\boldsymbol{k_{+A}}$ of 8.39 ± 0.16 μM^{-1} s^{-1} and $\boldsymbol{k_{+DA}}$ of 5.98 ± 0.19 μM^{-1} s^{-1} in the absence and presence of ADP, respectively (Fig. 4*A*). The dissociation rate constants $\boldsymbol{k_{-A}}$ and $\boldsymbol{k_{-DA}}$ are close to 0 and do not allow for a firm determination of the respective parameters (Fig. 4*A*). M5B^{S1} does not significantly quench pyrene fluorescence upon binding to pyrene-labeled F-actin. This observation precludes the use of this fluorescence label to directly determine the F-actin affinities in the presence and absence of ADP and the F-actin release rate constants, respectively. It is of note that the inability of M5B^{S1} to quench pyrene fluorescence is not an indication that the actomyosin complex is not formed, because a light scattering signal is observed under identical assay conditions (Fig. 4*A*, *inset*). Concomitantly, we find that the actoM5B^{S1} complex is formed under identical buffer conditions in high-speed cosedimentation assays (Fig. 5*B*).

Duty ratio of M5B^{S1}

The steady-state and transient kinetic characterization of single-headed M5B^{S1} allowed us to calculation the duty ratio, the time of its kinetic cycle M5B^{S1} spends strongly bound to actin (Fig. 1*B*). Values of ~0.46–0.6 were obtained with the following equation

Table 2
Transient state kinetic parameters of mouse M5B^{S1} in comparison with previously characterized class-5 myosins
Numbering of the kinetic constants refers to Fig. 1*B*. ND, not determined. NA, not experimentally accessible.

Parameter	Signal or calculation[a]	*Mm* M5B^{S1}	*Gg* M5A^{S1} (35)	*Hs* M5C^{S1} (16)	*Dm* M5^{S1} (47)
ATP interaction					
K_1k_{+2} (μM^{-1} s^{-1})	Tryptophan	0.39 ± 0.01	1.6 ± 0.2	ND	1.31 ± 0.52
K_1k_{+2} (μM^{-1} s^{-1})	mantATP	0.40 ± 0.01	1.5 ± 0.2	ND	1.31 ± 0.52
$1/K_{0.5}$ (μM)	Tryptophan	225.1 ± 14.7	ND	ND	ND
$k_3 + k_{-3}$ (s^{-1})	Tryptophan	85.4 ± 1.4	750 ± 45	90	68 ± 4.7
K_1k_{+2} (μM^{-1} s^{-1})	Light scattering	0.28 ± 0.01	0.9	0.82 ± 0.03	0.36 ± 0.006
$1/K_{0.5}$ (μM)	Light scattering	745.6 ± 120.7	ND	ND	>500
k_{+2} (s^{-1})	Light scattering	373.5 ± 18.7	870	287	>180
ADP interaction					
k_{+D} (μM^{-1} s^{-1})	mantADP	3.05 ± 0.16	4.6	ND	2.2 ± 0.3
k_{-D} (s^{-1})	mantADP[b]	14.3 ± 1.61	ND	ND	37.9 ± 2.4
k_{-D} (s^{-1})	mantADP[c]	18.0 ± 0.29	1.2	ND	38.3 ± 5.7
k_{-D} (s^{-1})	Tryptophan[c]	18.9 ± 0.09	ND	ND	ND
K_D (μM)	k_{-D}/k_{+D}	4.7–6.2	0.27	ND	17
k_{+D} (μM^{-1} s^{-1})	mantADP	2.71 ± 0.11	12.6	56–72	4.7
k_{-AD} (s^{-1})	mantADP[b]	21.9 ± 0.9	ND	ND	ND
k_{-AD} (s^{-1})	Light scattering[c]	17.13 ± 0.14	16	15.8 ± 0.8	ND
k_{-AD} (s^{-1})	mantADP[c]	16.69 ± 0.11	12	15.6 ± 0.6	150
K_{AD} (μM)	k_{-AD}/k_{+AD}	6.1–8.1	0.93	0.25 ± 0.02	32.54
Actin interaction					
k_{+A} (μM^{-1} s^{-1})	Light scattering[d]	8.39 ± 0.16	73	0.66 ± 0.02	2.5 ± 0.29
k_{-A} (s^{-1})	Pyrene-actin[d]	NA	0.00036	0.019	0.04 ± 0.001
K_A (nM)	k_{-A}/k_{+A}	NA	ND	29	16
k_{+AD} (μM^{-1} s^{-1})	Light scattering	5.98 ± 0.19	4.2	1.17 ± 0.03	2.3 ± 0.14
k_{-AD} (s^{-1})	Pyrene-actin[d]	NA	0.032	0.051	0.43 ± 0.01
K_{AD} (nM)	k_{-AD}/k_{+AD}	NA	ND	0.044	190

[a] In this study.
[b] From *y* intercept.
[c] From chasing experiment.
[d] Samples were treated with apyrase prior to the assay.

$$\text{duty ratio M5B}^{S1} = \frac{k_{cat}}{\boldsymbol{k_{-AD}}} \quad \text{(Eq. 7)}$$

based on the determined kinetic constants $\boldsymbol{k_{-AD}}$ = 16.69 ± 0.11–21.9 ± 0.9 s^{-1} and k_{cat} = 10.0 ± 0.1 s^{-1} (Tables 1 and 2) under saturating conditions. It is of note that this equation neglects that the duty ratio depends on [F-actin] and the [ATP] concentration (29, 33, 34).

The duty ratio values obtained for M5B^{S1} are lower than for single-headed constructs of other myosin-5 paralogs and unconventional myosins associated with cellular transport function (35–37). A duty ratio >0.5/head is a theoretical cutoff value and a minimum requirement for processivity, but duty ratios >0.95 are required for efficient single molecule processivity of a double-headed myosin (11, 35, 38). Calculation of the duty ratio of a myosin-5B dimer (39, 40) based on

$$\text{duty ratio M5B}^{HMM} = 1 - (1 - \text{duty ratio M5B}^{S1})^2 \quad \text{(Eq. 8)}$$

neglecting any steric factors, gating, and strain between the two motor domains results in values of 0.71–0.84.

Steady-state kinetic properties and key transient-state kinetic parameters of M5B^{HMM}

The steady- and transient-state kinetic parameters of M5B^{S1} measured in the absence of load indicate that the motor is unlikely to function as an efficient cargo transporter inside cells (Tables 1 and 2). This finding conflicts with the described physiological function of myosin-5B as transporter of membrane vesicles along the F-actin cytoskeleton (4, 19–21). We therefore tested whether a second head, as it is found in the myosin-5B dimer inside the cell, would change the enzymatic signatures and render the molecule a high-duty ratio motor. First, we measured the kinetic properties of M5B^{HMM} under steady-state conditions. F-actin activates the basal ATPase activity k_{basal} from 0.12 ± 0.02 s^{-1} ~65-fold to a maximum k_{cat} value of 7.91 ± 0.15 s^{-1} per head (Fig. 5*A*), a 20% reduction in k_{cat} when compared with M5B^{S1} (Tables 2 and 3). The K_{app} is with 3.12 ± 0.26 μM 60% lower than the respective parameter obtained with M5B^{S1}, the catalytic efficiency k_{cat}/K_{app} with ~2.5 elevated (Tables 1 and 3).

The difference in k_{cat} must be reflected in a transient kinetic parameter that rate-limits the actomyosin ATPase cycle and led us to test whether the presence of a second head would influence the ADP release rate from M5B^{HMM}. As shown in Fig. 5*B*, the ADP release rate from M5B^{HMM} in the presence of a 320-fold molar excess ADP (k_{-D} = 19.53 ± 0.25 s^{-1}; Fig. 5*B*) is identical to the parameter measured for single-headed M5B^{S1} (k_{-D} = 18.9 ± 0.09 s^{-1}) in the absence of F-actin (Fig. 3*D* and Table 2). Moreover, the fluorescence transient is best described by a single exponential, indicating that the presence of a second head *per se* does not affect the kinetics in the absence of F-actin. When bound to F-actin, the ADP release rate from M5B^{HMM} and the transient change in light scattering signal is double exponential with a fast rate $\boldsymbol{k_{-AD,HMM,fast}}$ of 7.24 s^{-1} and a slow phase $\boldsymbol{k_{-AD,HMM,slow}}$ of 1.27 s^{-1} (Fig. 5*C*). The fast rate is in good agreement with the titrated k_{cat} of 7.91 ± 0.15 s^{-1} obtained in the steady-state ATPase assay (Fig. 5*A* and Table 3) and probably represents the ADP release rate from the positively strained trail head, and the slow rate probably represents the ADP release rate from the negatively strained lead head (18). Taken together, the steady-state and transient-state

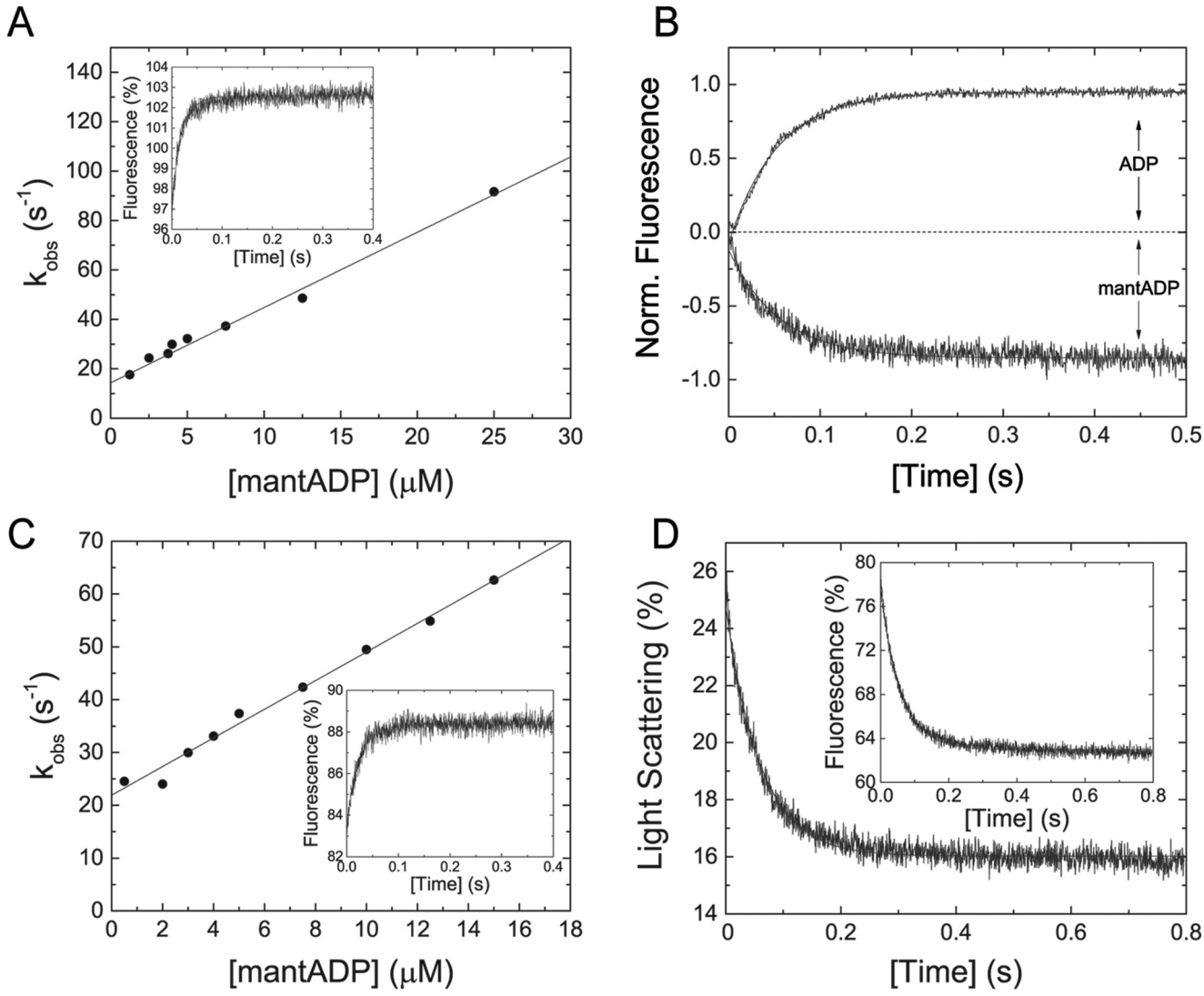

Figure 3. Transient kinetic interaction between M5^{S1} and actoM5^{S1} with ADP and ADP analogs. *A*, the observed rate constants upon rapidly mixing M5B^{S1} and mantADP follow a linear dependence in the concentration range tested. The *straight line* describes the second-order rate constant for ADP-binding k_{+D} to 3.05 ± 0.16 μM^{-1} s^{-1}. From the *y* intercept, the ADP release rate k_{-D} was determined to be 14.3 ± 1.61 s^{-1}. *Inset*, representative fluorescence increase after mixing 0.5 μM M5B^{S1} and 12.5 μM mantADP in a stopped-flow spectrophotometer. Single exponential fit to the transient results in a k_{obs} of 48.65 s^{-1}. *B*, ADP release kinetics from M5B^{S1}. Shown are the normalized data of the time-dependent increase in the intrinsic fluorescence signal after mixing 0.5 μM M5B^{S1} in the presence of a 25 μM ADP with 1.5 mM ATP. The transient was fit to a single exponential, yielding the ADP release rate constant k_{-D} = 18.9 s^{-1}. Similar, rapidly mixing 0.5 μM M5B^{S1} in the presence of a 50-fold molar excess of ADP (5 μM mantADP and 20 μM ADP) with 1.5 mM ATP resulted in a k_{-D} of 18.0 s^{-1}. *C*, mantADP dependence of the observed rate constant k_{obs} after mixing with actoM5B^{S1} under pseudo-first order conditions. The *solid line* describes the second-order binding rate constant $\boldsymbol{k_{+AD}}$ = 2.71 ± 0.11 μM^{-1} s^{-1} and the ADP release rate constant $\boldsymbol{k_{-AD}}$ = 21.9 ± 0.9 s^{-1}. *Inset*, time-dependent fluorescence increase after mixing 0.5 μM actoM5B^{S1} with 7.5 μM mantADP. Single exponential fit yields a k_{obs} = 42.39 s^{-1}. *D*, dissociation of 0.5 μM actomyosin in the presence of 40 μM ADP with 2 mM ATP. A single exponential fit to the time course of the light scattering signal yields a $\boldsymbol{k_{-AD}}$ of 17.13 s^{-1}. *Inset*, representative transient of the interaction between 0.5 μM actomyosin and 40 μM ADP (2.5 μM mantADP and 37.5 μM ADP) with 2 mM ATP. A $\boldsymbol{k_{-AD}}$ of 16.69 s^{-1} was determined from a single exponential fit to the data.

kinetic experiments indicate that the actin-activated ADP rate-limits the M5B^{HMM} but not the M5B^{S1} kinetic cycle. Accordingly, the duty ratio of the lead head is high and approaches unity based on the calculation according to Equation 7 with the measured rates $\boldsymbol{k_{-AD,HMM,fast}}$ = 7.24 ± 0.1 s^{-1} and k_{cat} = 7.91 ± 0.15 s^{-1}.

Chemical inhibition of M5B^{S1} with myoVin-1

Our detailed kinetic characterization of M5B^{S1} and M5B^{HMM} allowed us to probe the effect of the small molecule inhibitor myoVin-1 on its mechanoenzymatic properties. The pyrazolopyrimidine compound (Fig. 6*A*) was previously identified as an uncompetitive inhibitor for myosins-5A *in vitro* and has been used in cell biological studies to probe for myosin-5 motor function (41–45). To address whether the small molecule has selectivity for myosin-5A, we measured its effect in the actin-activated steady-state ATPase activity of M5B^{S1}. The addition of myoVin-1 to M5B^{S1} leads to a partial inhibition of the steady-state ATPase activity at a fixed F-actin concentration of 30 μM. The K_I, obtained after fitting the data, normalized to the ATPase activity in the absence of inhibitor, to a dose-response function is 23.12 ± 2.07 μM.

To address whether the partial reduction in the steady-state ATPase activity is caused by a decrease in k_{cat} or K_{app}, we measured the ATPase activity of M5B^{S1} as a function of [F-actin] at increasing myoVin-1 concentrations up to 30 μM. Higher

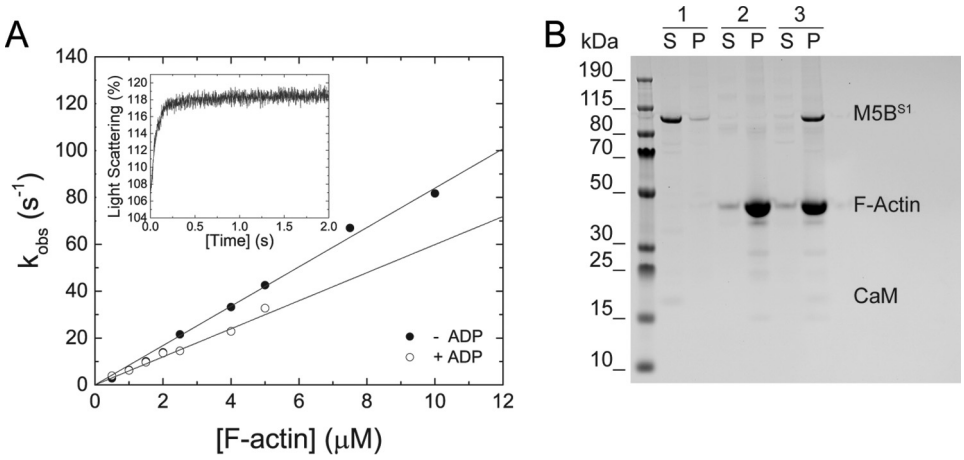

Figure 4. Transient kinetic interaction between M5B^{S1} and F-actin in the presence and absence of ADP. *A*, increasing concentrations of F-actin were mixed with M5B^{S1} in a stopped-flow spectrophotometer in the presence or absence of saturating ADP. Linear fits to the data sets describe the second-order binding rate constants k_{+A} and k_{+DA} to 8.39 ± 0.16 and 5.98 ± 0.19 μM^{-1} s^{-1}, respectively. *Inset*, time-dependent change in light scattering after rapidly mixing 0.5 μM M5B^{S1} with 4 μM F-actin in the presence of 80 μM ADP. Single exponential fit to the data set results in a k_{obs} of 13.6 s^{-1}. *B*, a cosedimentation assay shows that an actomyosin complex is formed in SF buffer. *Sample 1*, 2 μM M5B^{S1} (control); *sample 2*, 10 μM F-actin (control); *sample 3*, 2 μM M5B^{S1} and 10 μM F-actin. Abbreviations *S* and *P* refer to supernatant and pellet, respectively.

inhibitor concentrations resulted in precipitation in the presence of high F-actin concentrations. MyoVin-1 inhibits the actin-activated ATPase activity of M5B^{S1} in a dose-dependent manner by reducing k_{cat} (Fig. 6, *B* and *C*). The almost linear dependence of the ATPase activity on [F-actin] at high concentrations of myoVin-1 additionally suggests that the compound causes an increase in K_{app} and k_{cat} (Fig. 6, *B* and *C*).

Next, we tested whether myoVin-1 would inhibit the speed of actin filament gliding over a M5B^{HMM}-decorated surface in the *in vitro* motility assay. M5B^{HMM} smoothly moves actin filaments with a speed of 354 ± 119 nm s^{-1}. The presence of 500 μM myoVin-1 reduces the gliding speed to 201 ± 97 nm s^{-1} without completely inhibiting the motion, and many actin filaments move less regularly with periods of pauses (Fig. 6*C*). This observation is in line with the increased K_{app} observed in steady-state kinetic assays and suggests that the actin-activated ADP release is reduced in the presence of the compound (Fig. 6, *B* and *C*).

To investigate in more detail the transient kinetic transitions that are modulated by myoVin-1, we performed single-turnover measurements. By rapidly mixing M5B^{S1} with substoichiometric concentrations of mantATP, the molecular events of nucleotide binding, hydrolysis, and the release of the hydrolysis products can be monitored by the fluorescence increase, plateau, and decrease of the mant moiety. As shown in Fig. 6*D*, myoVin-1 predominantly reduces the release of mantADP in a concentration-dependent manner.

To explore how myoVin-1 modulates M5B^{S1} motor activity at the structural level, we performed *in silico* blind docking for unbiased mapping of the binding site and binding patterns in a homology model of the human myosin-5B motor domain with Mg·ADP·VO_4 in the active site. The nucleotide analog was included to account for the noncompetitive mode of action of myoVin-1. Of the top 10 ranked binding conformations, 7 ligands clustered near and around the relay helix, the thiol-reactive region (SH1–SH2), three of the seven-stranded β-sheets of the transducer, and the converter region of the myosin motor domain (Fig. 6, *E* and *F*) at a distance of 17 Å from the active site. The close-up view of energetically most favorable binding pose (binding energy = −10.5 kcal/mol) of myoVin-1 shows that the ligand interacts closely with interfaces formed by the seven-stranded β-sheets of the transducer on one side and hydrophobic residues including Trp-697 from the converter and the hydrophobic methylene group of Arg-152. The pyrazolopyrimidine group of myoVin-1 is further stabilized by Gln-149 of the α-helix that connects the seven-stranded β-sheet transducer (Fig. 6*F*). The predicted binding site in great distance to the active site supports previous reports that identified myoVin-1 as an uncompetitive myosin inhibitor (41).

Discussion

We chose to determine the kinetic and regulatory features of mammalian myosin-5B with single-headed and double-headed constructs that contain the entire neck domain with its six IQ motifs (Fig. 1*A*). The M5B^{S1} construct is therefore considerably longer than the myosin-5 constructs commonly studied (16, 35, 46–48). We chose this approach because recent studies indicate that the light chains bound to the myosin neck region are (i) not passive components of the holoenzyme, (ii) can directly interact with the myosin motor domain and each other in some cases, and (iii) may therefore directly influence myosin motor function (29, 30). Moreover, the length of the neck domain, which defines the number of IQ motifs in the myosin heavy chain, determines the kinetic and mechanical activity of the protein when artificially altered (49–51). The M5B^{S1} construct with its six IQ motifs allows a direct comparison between with the single-headed and double-headed myosin constructs and the contribution of a second head on myosin motor function and intramolecular gating. Moreover, our detailed kinetic characterization allows for the comparative analysis of kinetic signatures in the class 5 myosome, the description of the interaction of myosin-5B with the small molecule inhibitor myoVin-1, and the prediction of the impact of disease-causing mutations on myosin-5B motor function.

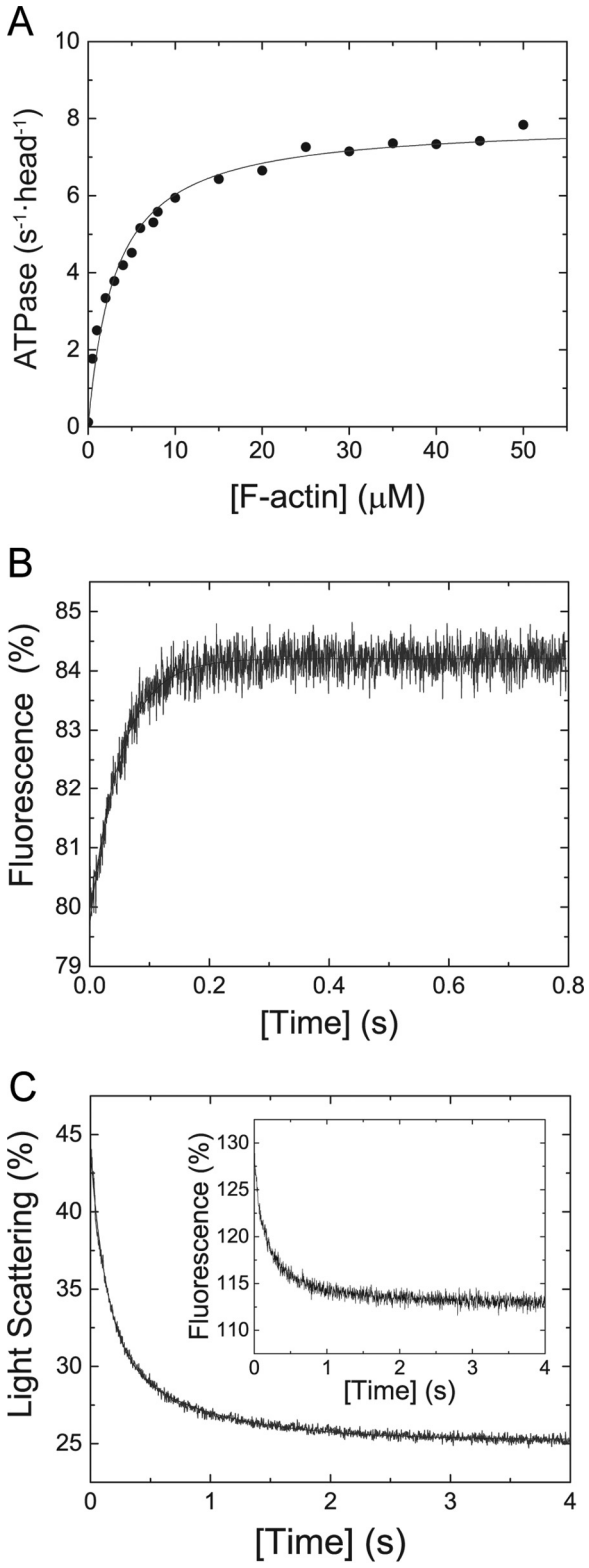

Figure 5. Steady-state ATPase activity and key kinetic parameters of M5B^{HMM}. *A*, the Michaelis–Menten parameters k_{cat} = 7.91 ± 0.15 s^{-1} and K_{app} = 3.12 ± 0.26 μM for M5B^{HMM} were determined under steady-state conditions for M5B^{HMM}. *B*, the transient fluorescence increase shows the interaction of 0.25 μM M5B^{HMM} in the presence of 80 μM ADP after rapid mixing with 2 mM ATP. Single exponential fit to the data set yields a $k_{-D,HMM}$ of 19.53 s^{-1}. *C*, dissociation of the actoM5B^{HMM}·ADP complex (0.25 μM M5B^{HMM}, 0.5 μM F-actin, 40 μM ADP) with 2 mM ATP results in a double-exponential decrease in light scattering signal ($\boldsymbol{k_{-AD,HMM,fast}}$ = 7.24 s^{-1}, $\boldsymbol{k_{-AD,HMM,slow}}$ = 1.27 s^{-1}). The fast phase has an amplitude of −12.4%, the slow phase an amplitude of −6.19%. *Inset*, similar ADP release rates and amplitudes ($\boldsymbol{k_{-AD,HMM,fast}}$ = 7.1 s^{-1}, $\boldsymbol{k_{-AD,HMM,slow}}$ = 1.1 s^{-1}, A_{fast} = −10.67%, A_{slow} = −4.4%) are obtained after rapidly mixing the actoM5B^{HMM}·mADP complex (0.25 μM M5B^{HMM}, 0.5 μM F-actin, 1.25 μM mADP, 18.75 μM ADP) with 1 mM ATP.

Steady-state and transient kinetic signatures of M5B^{S1}

With thorough transient and steady-state kinetic assays, we show that myosin-5B is a *bona fide* actin-based molecular motor with a high actin-activated ATPase activity under steady-state conditions. The transient kinetic signatures of M5B^{S1} include low thermodynamic ($\boldsymbol{K_{AD}}/K_D$ = ~1–1.7) and kinetic coupling ratios ($\boldsymbol{k_{-AD}}/k_{-D}$ = ~1–1.5), a high $\boldsymbol{k_{+AD}}/\boldsymbol{K_1k_{+2}}$ = ~10 ratio, and an intermediate duty ratio of ~0.46–0.6 (Table 2). Other characteristics of the M5B^{S1} ATPase cycle are a low $k_{cat}/\boldsymbol{k_{+2}}$ ratio of 0.027 that favors the dissociation of the actomyosin complex and a catalytic efficiency of k_{cat}/K_{app} ~0.8 μM^{-1} s^{-1} that indicates a low number of ATP turnovers per F-actin encounter (48). The kinetic signatures of M5B^{S1} indicate that the molecule has an intermediate duty ratio, in between the parameters determined for the nonprocessive M5C^{S1} and the processive M5A^{S1} (Tables 1 and 2).

Our results disagree to some extent with an initial report on the kinetic properties of human myosin-5B (52). Although this study did not include a detailed description of the myosin kinetic cycle in the actin-detached states and the interaction of M5B^{S1} with F-actin, we find that the presented second-order binding rate constants for ATP and the Michaelis–Menten parameter of the steady-state ATPase activity agree with the parameters determined in this study (52). Discrepancies were found in the nucleotide release rates that are slightly reduced when compared with our work and result in a higher duty ratio for a single-headed M5B^{S1} construct (52). In summary, the kinetic characteristics of M5B^{S1} presented in this study suggest that myosin-5B has a limited processive ability and is likely to work in an ensemble of motors to efficiently transport vesicles along the cellular F-actin cytoskeleton.

The second head in M5B^{HMM} establishes the kinetic prerequisite for single molecule processivity

Single molecule processivity is a feature of higher eukaryotic myosins-5A (17, 18). This behavior is in striking contrast to mammalian myosin-5C, *Drosophila* myosin-5, and the *Saccharomyces* myosins-5 Myo2p and Myo4p that have mechanoenzymatic properties that do not support single molecule processivity in biochemical *in vitro* assays (16, 47, 53). To either power or maximize the efficiency of myosin-5–based transport functions in the three-dimensional actin cytoskeleton of a cell, the motors cluster on the surface of cargo vesicles in densities up to >100 molecules to establish processivity (1, 54). This number may be crucial to maintain trafficking function, especially to compensate for either a reduced number of myosins-5 resulting in low surface densities or motors with compromised mechanoenzymatic activity as they are found in some disease states (32, 55). This makes the information regarding whether the myosin-5B dimer possesses the kinetic prerequisites for single molecule processivity essential to understand its function in normalcy and pathology.

Table 3
Steady-state and key transient-state kinetic parameters of mouse M5B^{HMM} in comparison with previously characterized class-5 myosins
Numbering of the transient-state kinetic constants refers to Fig. 1*B*. ND, not determined.

Parameter	Signal or calculation[a]	*Mm* M5B^{HMM}	*Mm/Gg* M5A^{HMM} (80, 81)	*Hs* M5C^{HMM} (15)	*Dm* M5^{HMM} (47)
Steady-state ATPase					
k_{basal} (s^{-1})	NADH assay	0.12 ± 0.02	ND	ND	ND
k_{cat} (s^{-1})	NADH assay	7.91 ± 0.15	3.8 ± 0.6	2.31 ± 0.55	12.6 ± 0.5
K_{app} (μM)	NADH assay	3.12 ± 0.26	0.15 ± 0.06	5.1 ± 1.8	10.8 ± 1.2
k_{cat}/K_{app} (μM^{-1} s^{-1})	NADH assay	~2.5	~25	~0.45	~1.2
ADP interaction					
$k_{-D,HMM}$ (s^{-1})	ADP[b]	19.53 ± 0.25	ND	ND	ND
$\boldsymbol{k_{-AD,HMM,fast}}$ (s^{-1})	Light scattering[b]	7.24 ± 0.1	42 ± 9	5.5 ± 0.2	ND
$\boldsymbol{k_{-AD,HMM,slow}}$ (s^{-1})	Light scattering[b]	1.27 ± 0.02	ND	0.026 ± 0.9	ND

[a] In this study.
[b] From chasing experiment.

To address the question of whether mammalian myosin-5B has the kinetic prerequisites to establish single molecule processivity, we explored the kinetic properties of double-headed M5B^{HMM}. The presence of a second head induces gating in the dimer that reduces the actin-activated ADP release rate $\boldsymbol{k_{-AD}}$ of ~65% and the k_{cat} of ~20% when compared with M5B^{S1} under identical assay conditions (Tables 1–3). Our transient and steady-state kinetic ensemble measurements further indicate that the ADP release is most likely not the rate-limiting step in the M5B^{S1} kinetic cycle but the rate-limiting step in the M5B^{HMM} kinetic cycle. This observation highlights that a second head in M5B^{HMM} influences the kinetics of the first head, as has been shown for the gating between the two heads of other unconventional myosins associated with transport function (18, 56–59).

As reported previously, myosins that move processively, either as dimers or as filaments, typically have a calculated duty ratio >0.95 (35, 38). Based on our duty ratio calculations on M5B^{HMM} that neglect every form of communication and steric constraints between the two heads, we speculate that the myosin-5B dimer is weakly processive and that a higher duty ratio and hence robust processivity may be achieved in the presence of actin-binding proteins or when stain is induced by a vesicle load. Both regulatory effects on the mechanical processivity have been described for some myosins-5, including nonprocessive myosins-5, and will be addressed for myosin-5B in future studies (60–63).

Potential impact of disease-associated mutations in the myosin-5B motor domain

14 mutations in *MYO5B* result in amino acid changes in the motor domain at the protein level (26). To explore the possible effect of these mutations on myosin motor function, we predicted the functional impact of the mutations, mapped the mutations in a homology model of myosin-5B, and linked the structural analysis to our kinetic data (64).

The functional impact score of the mutations is shown in Fig. 7*A*, the respective location in the myosin motor domain in Fig. 7*B*. Of the 14 mutations, 2 have low, 2 have medium, and 10 have high functional impact scores (Fig. 7*A*), thereby ranking their predicted impact on myosin motor function (64). The mutations are distributed throughout the entire myosin motor domain including the active site (G168R/R219H) and the actin-binding region (C514R/R531W/P619L) (Fig. 7*B*). The other mutations are located outside the functional structural elements in allosteric regions of the motor domain: mutations V108G, G316R, R401H, N456S, and R656C were previously attributed to play crucial roles in allosteric communication pathways in the myosin motor domain, whereas mutations G143R, G435(R/E), and R656C are predicted to induce protein instability and misfolding (26).

Among the mutations with a medium or high functional impact score are G168R and R219H in the conserved P-loop and switch-1 loop in the myosin active site. Both structural elements play crucial roles in the coordination of the nucleotide throughout the myosin kinetic cycle (Fig. 1*B*). Switch-1 mutations at equivalent positions to the highly conserved Arg-219 have previously been described to reduce the actin-activated ATPase activity and motile properties of class 5 and 2 myosins by interfering with the hydrolysis of ATP (65–67). The resulting low-duty ratio motors are expected to have a reduced processivity when compared with the wild-type protein. This property may be of physiological significance in the myosin-5B R219H mutant that, based on our kinetic characterization of the wild-type protein, is not expected to have robust single molecule processivity. A reduction in duty ratio and processivity may be reflected in the aberrant vesicle trafficking and segregation patterns in patients with microvillus inclusion disease.

Similarly, the replacement of a negatively charged with a bulky residue in the myosin-5B mutant R531W is expected to weaken the interaction with the actin filament that prominently involves electrostatic interactions between positively charges residues in the myosin motor domain and the negatively charged surface of the actin filament. A reduced F-actin interaction is expected to weaken the affinity of the motor domain for its track in the presence of ATP, thereby limiting the degree of processivity (59).

Why does myosin-5B binding not quench the fluorescence of pyrene-labeled F-actin?

Apart from a kinetic description of single- and double-headed myosin-5B constructs, this study revealed that the motor does not significantly quench pyrene fluorescence in transient-kinetic *in vitro* assays. Site-specific labeling of actin on Cys-374 is a powerful method to measure binding of most myosins to F-actin (68–71). Cys-374 is located on the surface of the actin subunit of a filament in the vicinity of the myosin-binding site. The fluorescence of pyrene-actin is only quenched when myosin binds in the strong binding state (AM or AM·ADP; Fig. 1*B*), but not in the weak binding state (AM·ATP

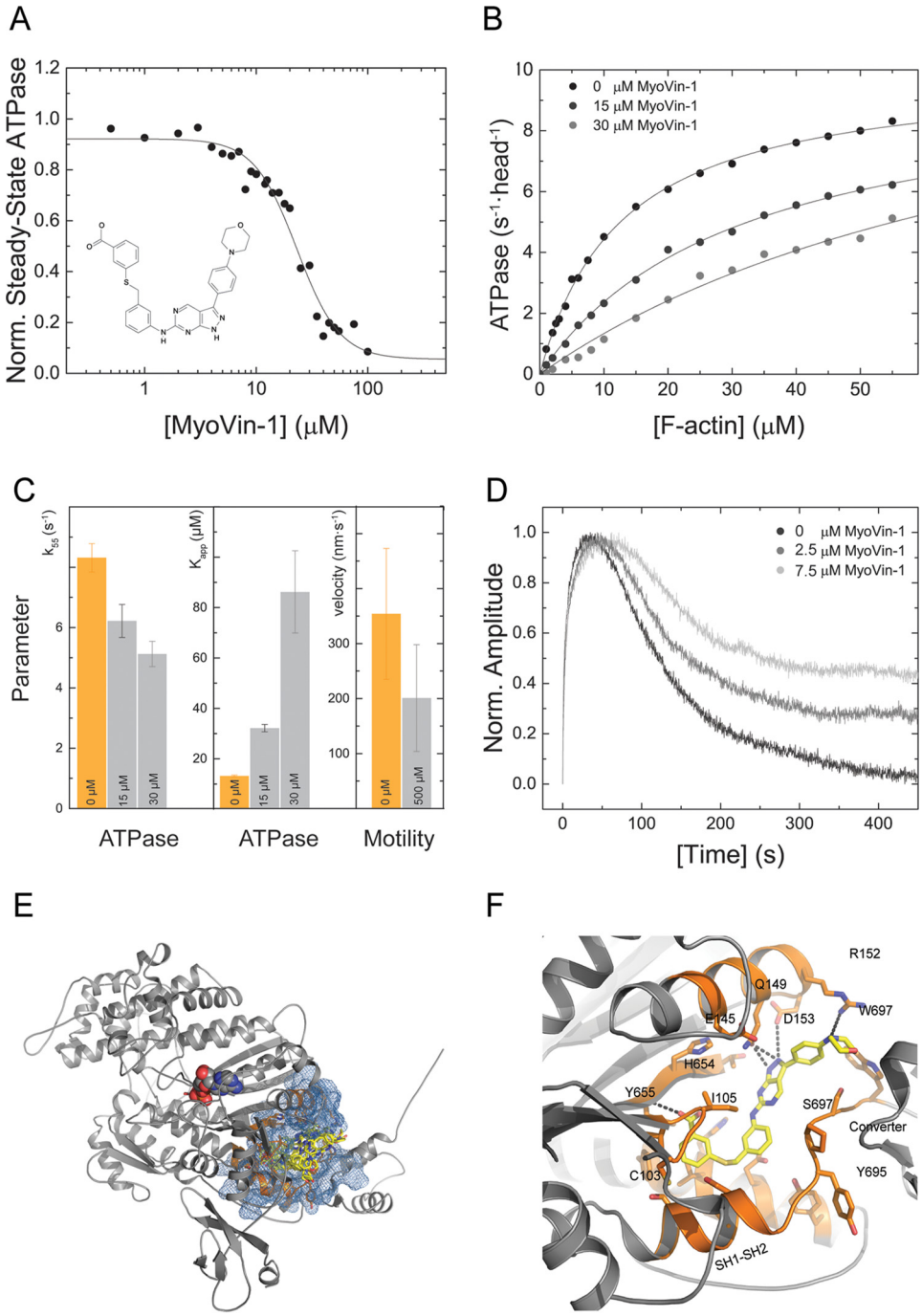

Figure 6. Chemical inhibition of M5B^{S1} with the small molecule myoVin-1. *A*, myoVin-1 inhibits the steady-state ATPase activity of M5B^{S1} at a fixed actin concentration of 30 μM in a dose-dependent manner with a K_I of 23.12 $\pm$ 2.07 μM. The data are normalized to the uninhibited control. The structure of the pyrazolopyrimidine compound myoVin-1 is shown in the *inset*. *B*, myoVin-1 changes the k_{cat} and the K_{app} of the M5B^{S1} actin-activated ATPase activity in a dose-dependent manner. *C*, effect of myoVin-1 on the steady-state ATPase activity of at 55 μM F-actin (k_{55}) and K_{app} of M5B^{S1} and gliding velocity. *Orange bars* represent the uninhibited control (0 μM myoVin-1). For k_{55} and K_{app}, *light gray bars* represent the measured parameters in the presence of 15 and 30 μM myoVin-1 as indicated. For the *in vitro* motility data, the *light gray bar* represents the actin gliding velocity in the presence of 500 μM myoVin-1 as indicated. *D*, single-turnover measurements (0.25 μM M5B^{S1} and 0.15 μM mantATP) in the presence of 0, 2.5, and 7.5 myoVin-1. The data show that myoVin-1 predominantly decreases the release of the mantATP hydrolysis products in a concentration-dependent manner. *E*, favorable binding pocket of myoVin-1 in the homology model of the human myosin-5B motor domain. The site is located at a distance of 17 Å to the nucleotide-binding pocket. The myosin-5B motor domain is shown in *gray cartoon* representation, the nucleotide is in *spheres*, and the predicted myoVin-1 binding pocket is in *orange*. The pharmacophore is highlighted in *blue*, and myoVin-1 is in *yellow stick* representation. The best pose has a binding energy of -10.5 kcal/mol. Of the 10 best scored poses, 8 ligands bind to the highlighted binding pocket and vary in their binding energy by only 1 kcal/mol. *F*, close-up view of the best binding conformation of myoVin-1 in the predicted binding pocket. The small molecule is coordinated by residues of the seven-stranded β-sheets of the transducer and hydrophobic residues including Trp-697 from the converter and hydrophobic methylene group of Arg-152. The pyrazolopyrimidine group of myoVin-1 is further stabilized by Gln-149 of the α-helix that connects the seven-stranded β-sheet transducer. *Color coding* is according to *E*.

A

Mutation	FIS	Impact	Location
V108G	4.16	high	
G143R	4.375	high	
G168R	4.16	high	Active site
R219H	3.465	medium	Active site
G316R	3.245	medium	
R401H	4.375	high	
G435R	4.11	high	
G435E	4.11	high	
N456S	4.105	high	
C514R	4.2	high	Actin interface
R531W	1.545	low	Actin interface
P619L	1.51	low	Actin interface
R656C	4.135	high	
P660L	4.51	high	

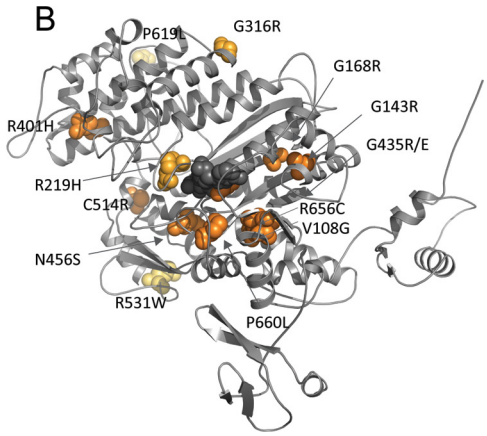

Figure 7. Location and impact of microvillus inclusion disease causing mutations in the myosin-5B motor domain. *A*, mutations in the myosin motor domain and their functional impact score and impact on myosin motor function. The localization to structural elements in the myosin motor domain to either the active site or the actin-binding region is indicated when applicable. *B*, the homology model of the human myosin-5B motor domain (*gray cartoon* representation) shows the localization of the respective disease-associated mutation. The mutations are colored according to severity from *yellow* to *orange* according to *A*. The nucleotide is highlighted in *gray spheres*. Mutations G168R and R219H are in the active site, and C514R/R531W/P619L is in the actin-binding region. Mutations V108G, G316R, R401H, N456S, and R656C are predicted to have allosteric effects on myosin motor function, whereas G143R, G435(R/E), and R656C may interfere with protein folding and induce protein instability (26).

and AM·ADP·P_i; Fig. 1*B*) (34). The light scattering signal in contrast can be used as readout for the binding of myosin to actin in both the strong and the weak states (34). Our observation that the interaction between $M5B^{S1}$ and pyrene-actin does not quench fluorescence but induces a change in light scattering signal further supports the results from the transient kinetic analysis that indicate that the motor binds F-actin weakly. However, actin sedimentation assays in the same buffer indicate that the actomyosin complex can form under the experimental conditions and that the lack of pyrene signal is caused by different interactions at the actomyosin interface when compared with other myosins-5. A similar result has been obtained for other myosins, including *Drosophila* indirect flight muscle myosin-2, rat myosin-9B, and also a truncated, single-headed myosin-5A construct (48, 72, 73).

Chemical inhibition with myoVin-1

The pyrazolopyrimidine compound myoVin-1 was identified as an uncompetitive inhibitor for myosin-5A based on privileged chemical scaffold design. The small molecule did not inhibit skeletal muscle myosin-2, nonmuscle myosin-2, and myosin-6 *in vitro*, suggesting selectivity for class 5 myosins (41). In this work, we show that myoVin-1 inhibits $M5B^{S1}$ (K_I = 23.12 ± 2.07 μM) with an almost identical K_I as a single-headed myosin-5A construct (K_I = 24 ± 4 μM) (41). Similar to the effects reported for myosin-5A, we find that myoVin-1 partially inhibits the actin-activated ATPase activity of $M5B^{S1}$ (41). Partial inhibition is also observed in the *in vitro* motility assay, suggesting that a decrease in the actin-activated ADP release is the kinetic step in the actomyosin mechanoenzymatic cycle that is altered in the presence of the small molecule compound.

MyoVin-1 has been used to inhibit the myosin-5B–dependent trafficking of podocalyxin to apical membrane insertion sites and myosin-5–dependent intersynaptic vesicle exchange in live cells (43, 44). Vesicle velocity and directionality are slightly reduced in the presence of myoVin-1, whereas the frequency of vesicle pausing increases (43). These quantitative *in vivo* results agree with the observed partial inhibition of the myosin ATPase activity and functional activity and the repetitive motion of actin filaments in the *in vitro* motility assay in this study (Fig. 5, *A–D*). Intriguingly, myosin-5 moves vesicles with a speed of 320 ± 80 nm s^{-1} *in vivo* that drops to 280 ± 60 nm s^{-1} in the presence of 30 μM myoVin-1 (43). This effect is very similar to the speeds measured in the *in vitro* motility assay (354 ± 119 nm s^{-1} (no myoVin-1); 201 ± 97 nm s^{-1} (500 μM myoVin-1) (Fig. 6*C*). It is also of note that myoVin-1 inhibits the activity of skeletal muscle myosin-2 in prothrombin activation, a finding that contrasts the above mentioned selectivity for class 5 myosins (74).

Based on our blind docking results, we predict the inhibitor binding pocket to be located near the converter region in the myosin motor domain (Fig. 6, *E* and *F*). The predicted binding pocket is remote from the active site, underlining the uncompetitive mode of inhibition of myoVin-1. Interestingly, the same pocket was recently identified in structural studies as the binding site for the myosin-2 inhibitor CK-571, suggesting that the converter/SH1-SH2/relay interface is a promising site to target myosin motor function with small molecules (75).

In summary, the inhibition of the kinetic and functional activity of myosin-5B constructs in biochemical *in vitro* assays at high inhibitor concentrations, together with the results of previous *in vitro* and *in vivo* studies, suggest that myoVin-1 is not a potent inhibitor of class 5 myosins. The lack of selectivity for a myosin-5 paralogs, the almost identical K_I values for myosins-5A and -5B *in vitro*, and the partial inhibition of the sliding velocity and steady-state ATPase activity of potentially all three mammalian myosins-5 in a cell suggest that caution should be used when interpreting the results from cell biological experiments in which myoVin-1 is used.

Experimental procedures

Construction of expression constructs, recombinant protein production, and preparation

cDNA constructs encoding for murine $M5B^{S1}$ (amino acids 1–906, molecular mass of 107 kDa) and $M5B^{HMM}$ (amino acids

1–1095, molecular mass of 127 kDa) were inserted in a modified pFastBac1 encoding for a C-terminal Flag tag with standard cloning techniques. Rat CaM cDNA (molecular mass of 17 kDa) that is at the protein level 100% identical with murine CaM was expressed from pFastBac1. Recombinant baculovirus generation and gene expression were performed as recommended by the manufacturer (Thermo Fisher Scientific). For protein production, *Sf*9 insect cells were infected with recombinant baculoviruses encoding $M5B^{S1}$/$M5B^{HMM}$ and CaM, and the protein complexes were purified as described via Flag capture (76). $M5B^{HMM}$ was further purified to electrophoretic homogeneity by size exclusion chromatography on a HiLoad Superdex 16/600 pg (GE Healthcare Life Sciences). Actin was prepared from rabbit skeletal muscle acetone powder (Pel-Freez Biologicals) and labeled with *N*-(1-prenyl)iodoacetamide (pyrene) as described (69, 77).

Steady-state and transient state kinetic assays

Steady-state kinetic assays were performed in a Cary 60 spectrophotometer (Agilent Technologies) at a temperature of 25 °C in buffer containing 10 mM MOPS, pH 7.0, 2 mM ATP, 50 mM NaCl, 2 mM $MgCl_2$, 0.15 mM EGTA, 40 units/ml L-lactic dehydrogenase, 200 units/ml pyruvate kinase, 200 μM NADH, and 1 mM phosphoenolpyruvate at a protein concentration of <50 nM $M5B^{S1}$ or $M5B^{HMM}$ as described (76). Transient kinetic assays were carried out on a Sf-61 DX2 stopped-flow (Hi-Tech Scientific) equipped with a 75-watt mercury–xenon arc lamp at a temperature of 20 °C in SF buffer containing 25 mM MOPS, pH 7.0, 100 mM KCl, 5 mM $MgCl_2$, and 0.1 mM EGTA unless stated otherwise. Concentrations throughout the text represent post-mixing concentrations. Light scattering was excited at a wavelength of 320 nm, and emission was measured at a fixed angle of 90°. The intrinsic tryptophan fluoresce was excited at a wavelength of 297 nm, and the emission was recorded after passage through a WG320 filter. The fluorescence of mant-nucleotides was either directly excited at a wavelength of 365 nm or indirectly after energy transfer from tryptophan residues, and the emission was detected after passage through a LP390 filter.

The small molecule myoVin-1 (Calbiochem) was diluted in DMSO to a concentration of 50 mg/ml (92.83 mM) and stored at −20 °C. Kinetic measurements in the presence of myoVin-1 were carried out at a constant concentration of 2% DMSO. Reaction mixtures were incubated for 10 min at room temperature protected from light prior to the assay.

Cosedimentation assay

Proteins (2 μM $M5B^{S1}$, 10 μM F-actin) were incubated in SF buffer for 10 min at room temperature. The samples were centrifuged (30 min, 100,000 × *g*, 4 °C), and supernatant and pellet fractions were separated on a 4–12% Bis-Tris gel (Thermo Scientific). The gel was stained with PageBlue (Thermo Scientific), destained with water, and documented on an Odyssey scanner (LI-COR Biosciences).

Functional in vitro motility assay

The *in vitro* motility assay was performed with $M5B^{HMM}$ as described previously in 20 mM MOPS, pH 7.4, 2 mM $MgCl_2$, 0.1 mM EGTA, 50 mM KCl, 1 mM ATP, 2.5 μg/ml glucose oxidase, 45 μg/ml catalase, 2.5 mg/ml glucose, and 50 mM DTT at a temperature of 30 °C (49).

In silico homology modeling and docking

The human myosin-5B motor domain (amino acids 1–767) was modeled using the human myosin-5C motor domain (Protein Data Bank code 4ZG4) pre-powerstroke state structure as a template. Both proteins share 68% sequence identity and 81% homology. The model was built using Modeler 9.18 (78). For the myoVin-1–binding site analysis, the human myosin-5B motor domain model bound to $Mg{\cdot}ADP{\cdot}VO_4$ was used for docking studies. AutodockTools was used to prepare the ligands and to assign Gasteiger charges (79). Blind docking was performed using autodock Vina by defining a cubic grid size of 79 Å. The exhaustiveness level was set at 50, and default options were used for the remaining parameters. The top 10 best docked ligand poses were selected based on the free energy predictions (−10.5 kcal/mol to −8.5 kcal/mol).

Author contributions—S. M. H. cloned expression plasmids, produced and purified proteins, and performed and analyzed the kinetic experiments. K. C. performed and analyzed the *in silico* homology modeling and docking studies. J. R. S. performed and analyzed the *in vitro* motility assay. All authors wrote and approved the final version of the manuscript.

References

1. Gross, S. P., Tuma, M. C., Deacon, S. W., Serpinskaya, A. S., Reilein, A. R., and Gelfand, V. I. (2002) Interactions and regulation of molecular motors in *Xenopus* melanophores. *J. Cell Biol.* **156,** 855–865
2. Hammer, J. A., 3rd, and Sellers, J. R. (2011) Walking to work: roles for class V myosins as cargo transporters. *Nat. Rev. Mol. Cell Biol.* **13,** 13–26
3. Jacobs, D. T., Weigert, R., Grode, K. D., Donaldson, J. G., and Cheney, R. E. (2009) Myosin Vc is a molecular motor that functions in secretory granule trafficking. *Mol. Biol. Cell* **20,** 4471–4488
4. Lapierre, L. A., Kumar, R., Hales, C. M., Navarre, J., Bhartur, S. G., Burnette, J. O., Provance, D. W., Jr., Mercer, J. A., Bähler, M., and Goldenring, J. R. (2001) Myosin vb is associated with plasma membrane recycling systems. *Mol. Biol. Cell* **12,** 1843–1857
5. Nascimento, A. A., Roland, J. T., and Gelfand, V. I. (2003) Pigment cells: a model for the study of organelle transport. *Annu. Rev. Cell Dev. Biol.* **19,** 469–491
6. Rodriguez, O. C., and Cheney, R. E. (2002) Human myosin-Vc is a novel class V myosin expressed in epithelial cells. *J. Cell Sci.* **115,** 991–1004
7. Wagner, W., Brenowitz, S. D., and Hammer, J. A., 3rd (2011) Myosin-Va transports the endoplasmic reticulum into the dendritic spines of Purkinje neurons. *Nat. Cell Biol.* **13,** 40–48
8. Wu, X., Rao, K., Bowers, M. B., Copeland, N. G., Jenkins, N. A., and Hammer, J. A., 3rd (2001) Rab27a enables myosin Va-dependent melanosome capture by recruiting the myosin to the organelle. *J. Cell Sci.* **114,** 1091–1100
9. Ji, H. H., Zhang, H. M., Shen, M., Yao, L. L., and Li, X. D. (2015) The motor function of *Drosophila melanogaster* myosin-5 is activated by calcium and cargo-binding protein dRab11. *Biochem. J.* **469,** 135–144
10. Johnston, G. C., Prendergast, J. A., and Singer, R. A. (1991) The *Saccharomyces cerevisiae* MYO2 gene encodes an essential myosin for vectorial transport of vesicles. *J. Cell Biol.* **113,** 539–551
11. Heissler, S. M., and Sellers, J. R. (2016) Kinetic adaptations of myosins for their diverse cellular functions. *Traffic* **17,** 839–859
12. Heissler, S. M., and Sellers, J. R. (2016) Various themes of myosin regulation. *J. Mol. Biol.* **428,** 1927–1946

13. Roland, J. T., Lapierre, L. A., and Goldenring, J. R. (2009) Alternative splicing in class V myosins determines association with Rab10. *J. Biol. Chem.* **284,** 1213–1223
14. Sladewski, T. E., Krementsova, E. B., and Trybus, K. M. (2016) Myosin Vc is specialized for transport on a secretory superhighway. *Curr. Biol.* **26,** 2202–2207
15. Gunther, L. K., Furuta, K., Bao, J., Urbanowski, M. K., Kojima, H., White, H. D., and Sakamoto, T. (2014) Coupling of two non-processive myosin 5c dimers enables processive stepping along actin filaments. *Sci. Rep.* **4,** 4907
16. Takagi, Y., Yang, Y., Fujiwara, I., Jacobs, D., Cheney, R. E., Sellers, J. R., and Kovács, M. (2008) Human myosin Vc is a low duty ratio, nonprocessive molecular motor. *J. Biol. Chem.* **283,** 8527–8537
17. Mehta, A. D., Rock, R. S., Rief, M., Spudich, J. A., Mooseker, M. S., and Cheney, R. E. (1999) Myosin-V is a processive actin-based motor. *Nature* **400,** 590–593
18. Sakamoto, T., Webb, M. R., Forgacs, E., White, H. D., and Sellers, J. R. (2008) Direct observation of the mechanochemical coupling in myosin Va during processive movement. *Nature* **455,** 128–132
19. Cheeseman, L. P., Boulanger, J., Bond, L. M., and Schuh, M. (2016) Two pathways regulate cortical granule translocation to prevent polyspermy in mouse oocytes. *Nat. Commun.* **7,** 13726
20. Knowles, B. C., Roland, J. T., Krishnan, M., Tyska, M. J., Lapierre, L. A., Dickman, P. S., Goldenring, J. R., and Shub, M. D. (2014) Myosin Vb uncoupling from RAB8A and RAB11A elicits microvillus inclusion disease. *J. Clin. Invest.* **124,** 2947–2962
21. Vogel, G. F., Klee, K. M., Janecke, A. R., Müller, T., Hess, M. W., and Huber, L. A. (2015) Cargo-selective apical exocytosis in epithelial cells is conducted by Myo5B, Slp4a, Vamp7, and Syntaxin 3. *J. Cell Biol.* **211,** 587–604
22. Liu, Y., Xu, X. H., Chen, Q., Wang, T., Deng, C. Y., Song, B. L., Du, J. L., and Luo, Z. G. (2013) Myosin Vb controls biogenesis of post-Golgi Rab10 carriers during axon development. *Nat. Commun.* **4,** 2005
23. Schuh, M. (2011) An actin-dependent mechanism for long-range vesicle transport. *Nat. Cell Biol.* **13,** 1431–1436
24. Wang, Z., Edwards, J. G., Riley, N., Provance, D. W., Jr., Karcher, R., Li, X. D., Davison, I. G., Ikebe, M., Mercer, J. A., Kauer, J. A., and Ehlers, M. D. (2008) Myosin Vb mobilizes recycling endosomes and AMPA receptors for postsynaptic plasticity. *Cell* **135,** 535–548
25. Roland, J. T., Bryant, D. M., Datta, A., Itzen, A., Mostov, K. E., and Goldenring, J. R. (2011) Rab GTPase-Myo5B complexes control membrane recycling and epithelial polarization. *Proc. Natl. Acad. Sci. U.S.A.* **108,** 2789–2794
26. van der Velde, K. J., Dhekne, H. S., Swertz, M. A., Sirigu, S., Ropars, V., Vinke, P. C., Rengaw, T., van den Akker, P. C., Rings, E. H., Houdusse, A., and van Ijzendoorn, S. C. (2013) An overview and online registry of microvillus inclusion disease patients and their MYO5B mutations. *Hum. Mutat.* **34,** 1597–1605
27. Müller, T., Hess, M. W., Schiefermeier, N., Pfaller, K., Ebner, H. L., Heinz-Erian, P., Ponstingl, H., Partsch, J., Röllinghoff, B., Köhler, H., Berger, T., Lenhartz, H., Schlenck, B., Houwen, R. J., Taylor, C. J., *et al.* (2008) MYO5B mutations cause microvillus inclusion disease and disrupt epithelial cell polarity. *Nat. Genet.* **40,** 1163–1165
28. Pylypenko, O., Attanda, W., Gauquelin, C., Lahmani, M., Coulibaly, D., Baron, B., Hoos, S., Titus, M. A., England, P., and Houdusse, A. M. (2013) Structural basis of myosin V Rab GTPase-dependent cargo recognition. *Proc. Natl. Acad. Sci. U.S.A.* **110,** 20443–20448
29. De La Cruz, E. M., Wells, A. L., Sweeney, H. L., and Ostap, E. M. (2000) Actin and light chain isoform dependence of myosin V kinetics. *Biochemistry* **39,** 14196–14202
30. Heissler, S. M., and Sellers, J. R. (2014) Myosin light chains: teaching old dogs new tricks. *Bioarchitecture* **4,** 169–188
31. Vogel, G. F., Janecke, A. R., Krainer, I. M., Gutleben, K., Witting, B., Mitton, S. G., Mansour, S., Ballauff, A., Roland, J. T., Engevik, A. C., Cutz, E., Müller, T., Goldenring, J. R., Huber, L. A., and Hess, M. W. (2017) Abnormal Rab11-Rab8-vesicles cluster in enterocytes of patients with microvillus inclusion disease. *Traffic* **18,** 453–464
32. Szperl, A. M., Golachowska, M. R., Bruinenberg, M., Prekeris, R., Thunnissen, A. M., Karrenbeld, A., Dijkstra, G., Hoekstra, D., Mercer, D., Ksiazyk, J., Wijmenga, C., Wapenaar, M. C., Rings, E. H., and van IJzendoorn, S. C. (2011) Functional characterization of mutations in the myosin Vb gene associated with microvillus inclusion disease. *J. Pediatr. Gastroenterol. Nutr.* **52,** 307–313
33. Henn, A., and De La Cruz, E. M. (2005) Vertebrate myosin VIIb is a high duty ratio motor adapted for generating and maintaining tension. *J. Biol. Chem.* **280,** 39665–39676
34. De La Cruz, E. M., and Ostap, E. M. (2009) Kinetic and equilibrium analysis of the myosin ATPase. *Methods Enzymol.* **455,** 157–192
35. De La Cruz, E. M., Wells, A. L., Rosenfeld, S. S., Ostap, E. M., and Sweeney, H. L. (1999) The kinetic mechanism of myosin V. *Proc. Natl. Acad. Sci. U.S.A.* **96,** 13726–13731
36. Heissler, S. M., and Manstein, D. J. (2012) Functional characterization of the human myosin-7a motor domain. *Cell Mol. Life Sci.* **69,** 299–311
37. Heissler, S. M., Selvadurai, J., Bond, L. M., Fedorov, R., Kendrick-Jones, J., Buss, F., and Manstein, D. J. (2012) Kinetic properties and small-molecule inhibition of human myosin-6. *FEBS Lett.* **586,** 3208–3214
38. Nagy, A., Takagi, Y., Billington, N., Sun, S. A., Hong, D. K., Homsher, E., Wang, A., and Sellers, J. R. (2013) Kinetic characterization of nonmuscle myosin IIb at the single molecule level. *J. Biol. Chem.* **288,** 709–722
39. Veigel, C., Wang, F., Bartoo, M. L., Sellers, J. R., and Molloy, J. E. (2002) The gated gait of the processive molecular motor, myosin V. *Nat. Cell Biol.* **4,** 59–65
40. Katsimitsoulia, Z., and Taylor, W. R. (2012) Coarse-grained simulation of myosin-V movement. *Comput. Math. Methods Med.* **2012,** 781456
41. Islam, K., Chin, H. F., Olivares, A. O., Saunders, L. P., De La Cruz, E. M., and Kapoor, T. M. (2010) A myosin V inhibitor based on privileged chemical scaffolds. *Angew. Chem. Int. Ed Engl.* **49,** 8484–8488
42. Avasthi, P., Onishi, M., Karpiak, J., Yamamoto, R., Mackinder, L., Jonikas, M. C., Sale, W. S., Shoichet, B., Pringle, J. R., and Marshall, W. F. (2014) Actin is required for IFT regulation in *Chlamydomonas reinhardtii*. *Curr. Biol.* **24,** 2025–2032
43. Gramlich, M. W., and Klyachko, V. A. (2017) Actin/myosin-V- and activity-dependent inter-synaptic vesicle exchange in central neurons. *Cell Rep.* **18,** 2096–2104
44. Richards, M., Hetheridge, C., and Mellor, H. (2015) The formin FMNL3 controls early apical specification in endothelial cells by regulating the polarized trafficking of podocalyxin. *Curr. Biol.* **25,** 2325–2331
45. Zorca, C. E., Kim, L. K., Kim, Y. J., Krause, M. R., Zenklusen, D., Spilianakis, C. G., and Flavell, R. A. (2015) Myosin VI regulates gene pairing and transcriptional pause release in T cells. *Proc. Natl. Acad. Sci. U.S.A.* **112,** E1587–E1593
46. Rosenfeld, S. S., Houdusse, A., and Sweeney, H. L. (2005) Magnesium regulates ADP dissociation from myosin V. *J. Biol. Chem.* **280,** 6072–6079
47. Tóth, J., Kovács, M., Wang, F., Nyitray, L., and Sellers, J. R. (2005) Myosin V from *Drosophila* reveals diversity of motor mechanisms within the myosin V family. *J. Biol. Chem.* **280,** 30594–30603
48. Trybus, K. M., Krementsova, E., and Freyzon, Y. (1999) Kinetic characterization of a monomeric unconventional myosin V construct. *J. Biol. Chem.* **274,** 27448–27456
49. Sakamoto, T., Wang, F., Schmitz, S., Xu, Y., Xu, Q., Molloy, J. E., Veigel, C., and Sellers, J. R. (2003) Neck length and processivity of myosin V. *J. Biol. Chem.* **278,** 29201–29207
50. Sakamoto, T., Yildez, A., Selvin, P. R., and Sellers, J. R. (2005) Step-size is determined by neck length in myosin V. *Biochemistry* **44,** 16203–16210
51. Moore, J. R., Krementsova, E. B., Trybus, K. M., and Warshaw, D. M. (2004) Does the myosin V neck region act as a lever? *J. Muscle Res. Cell Motil.* **25,** 29–35
52. Watanabe, S., Mabuchi, K., Ikebe, R., and Ikebe, M. (2006) Mechanoenzymatic characterization of human myosin Vb. *Biochemistry* **45,** 2729–2738
53. Reck-Peterson, S. L., Tyska, M. J., Novick, P. J., and Mooseker, M. S. (2001) The yeast class V myosins, Myo2p and Myo4p, are nonprocessive actin-based motors. *J. Cell Biol.* **153,** 1121–1126
54. Miller, K. E., and Sheetz, M. P. (2000) Characterization of myosin V binding to brain vesicles. *J. Biol. Chem.* **275,** 2598–2606
55. Dong, W., Chen, X., Chen, P., Yue, D., Zhu, L., and Fan, Q. (2012) Inactivation of MYO5B promotes invasion and motility in gastric cancer cells. *Dig. Dis. Sci.* **57,** 1247–1252

56. De La Cruz, E. M., Ostap, E. M., and Sweeney, H. L. (2001) Kinetic mechanism and regulation of myosin VI. *J. Biol. Chem.* **276,** 32373–32381
57. Ropars, V., Yang, Z., Isabet, T., Blanc, F., Zhou, K., Lin, T., Liu, X., Hissier, P., Samazan, F., Amigues, B., Yang, E. D., Park, H., Pylypenko, O., Cecchini, M., Sindelar, C. V., Sweeney, H. L., and Houdusse, A. (2016) The myosin X motor is optimized for movement on actin bundles. *Nat. Commun.* **7,** 12456
58. Forgacs, E., Cartwright, S., Sakamoto, T., Sellers, J. R., Corrie, J. E., Webb, M. R., and White, H. D. (2008) Kinetics of ADP dissociation from the trail and lead heads of actomyosin V following the power stroke. *J. Biol. Chem.* **283,** 766–773
59. Rosenfeld, S. S., and Sweeney, H. L. (2004) A model of myosin V processivity. *J. Biol. Chem.* **279,** 40100–40111
60. Bao, J., Huck, D., Gunther, L. K., Sellers, J. R., and Sakamoto, T. (2013) Actin structure-dependent stepping of myosin 5a and 10 during processive movement. *PLoS One* **8,** e74936
61. Clayton, J. E., Pollard, L. W., Sckolnick, M., Bookwalter, C. S., Hodges, A. R., Trybus, K. M., and Lord, M. (2014) Fission yeast tropomyosin specifies directed transport of myosin-V along actin cables. *Mol. Biol. Cell* **25,** 66–75
62. Hodges, A. R., Krementsova, E. B., Bookwalter, C. S., Fagnant, P. M., Sladewski, T. E., and Trybus, K. M. (2012) Tropomyosin is essential for processive movement of a class V myosin from budding yeast. *Curr. Biol.* **22,** 1410–1416
63. Sckolnick, M., Krementsova, E. B., Warshaw, D. M., and Trybus, K. M. (2016) Tropomyosin isoforms bias actin track selection by vertebrate myosin Va. *Mol. Biol. Cell* **27,** 2889–2897
64. Reva, B., Antipin, Y., and Sander, C. (2011) Predicting the functional impact of protein mutations: application to cancer genomics. *Nucleic Acids Res.* **39,** e118
65. Forgacs, E., Sakamoto, T., Cartwright, S., Belknap, B., Kovács, M., Tóth, J., Webb, M. R., Sellers, J. R., and White, H. D. (2009) Switch 1 mutation S217A converts myosin V into a low duty ratio motor. *J. Biol. Chem.* **284,** 2138–2149
66. Li, X. D., Rhodes, T. E., Ikebe, R., Kambara, T., White, H. D., and Ikebe, M. (1998) Effects of mutations in the γ-phosphate binding site of myosin on its motor function. *J. Biol. Chem.* **273,** 27404–27411
67. Shimada, T., Sasaki, N., Ohkura, R., and Sutoh, K. (1997) Alanine scanning mutagenesis of the switch I region in the ATPase site of *Dictyostelium discoideum* myosin II. *Biochemistry* **36,** 14037–14043
68. Adamek, N., and Geeves, M. A. (2014) Use of pyrene-labelled actin to probe actin-myosin interactions: kinetic and equilibrium studies. *EXS* **105,** 87–104
69. Criddle, A. H., Geeves, M. A., and Jeffries, T. (1985) The use of actin labelled with *N*-(1-pyrenyl)iodoacetamide to study the interaction of actin with myosin subfragments and troponin/tropomyosin. *Biochem. J.* **232,** 343–349
70. Geeves, M. A. (1989) Dynamic interaction between actin and myosin subfragment 1 in the presence of ADP. *Biochemistry* **28,** 5864–5871
71. Kouyama, T., and Mihashi, K. (1981) Fluorimetry study of *N*-(1-pyrenyl) iodoacetamide-labelled F-actin. Local structural change of actin protomer both on polymerization and on binding of heavy meromyosin. *Eur. J. Biochem.* **114,** 33–38
72. Nalavadi, V., Nyitrai, M., Bertolini, C., Adamek, N., Geeves, M. A., and Bähler, M. (2005) Kinetic mechanism of myosin IXB and the contributions of two class IX-specific regions. *J. Biol. Chem.* **280,** 38957–38968
73. Silva, R., Sparrow, J. C., and Geeves, M. A. (2003) Isolation and kinetic characterisation of myosin and myosin S1 from the *Drosophila* indirect flight muscles. *J. Muscle Res. Cell Motil.* **24,** 489–498
74. Deguchi, H., Sinha, R. K., Marchese, P., Ruggeri, Z. M., Zilberman-Rudenko, J., McCarty, O. J. T., Cohen, M. J., and Griffin, J. H. (2016) Prothrombotic skeletal muscle myosin directly enhances prothrombin activation by binding factors Xa and Va. *Blood* **128,** 1870–1878
75. Sirigu, S., Hartman, J. J., Planelles-Herrero, V. J., Ropars, V., Clancy, S., Wang, X., Chuang, G., Qian, X., Lu, P. P., Barrett, E., Rudolph, K., Royer, C., Morgan, B. P., Stura, E. A., Malik, F. I., *et al.* (2016) Highly selective inhibition of myosin motors provides the basis of potential therapeutic application. *Proc. Natl. Acad. Sci. U.S.A.* **113,** E7448–E7455
76. Heissler, S. M., Chinthalapudi, K., and Sellers, J. R. (2015) Kinetic characterization of the sole nonmuscle myosin-2 from the model organism *Drosophila melanogaster*. *FASEB J.* **29,** 1456–1466
77. Lehrer, S. S., and Kerwar, G. (1972) Intrinsic fluorescence of actin. *Biochemistry* **11,** 1211–1217
78. Sali, A., and Blundell, T. L. (1993) Comparative protein modelling by satisfaction of spatial restraints. *J. Mol. Biol.* **234,** 779–815
79. Morris, G. M., Huey, R., Lindstrom, W., Sanner, M. F., Belew, R. K., Goodsell, D. S., and Olson, A. J. (2009) AutoDock4 and AutoDockTools4: Automated docking with selective receptor flexibility. *J. Comput. Chem.* **30,** 2785–2791
80. Wang, F., Chen, L., Arcucci, O., Harvey, E. V., Bowers, B., Xu, Y., Hammer, J. A., 3rd, Sellers, J. R. (2000) Effect of ADP and ionic strength on the kinetic and motile properties of recombinant mouse myosin V. *J. Biol. Chem.* **275,** 4329–4335
81. Olivares, A. O., Chang, W., Mooseker, M. S., Hackney, D. D., and De La Cruz, E. M. (2006) The tail domain of myosin Va modulates actin binding to one head. *J. Biol. Chem.* **281,** 31326–31336